Review Article

Mario Barbatti*

When theory came first: a review of theoretical chemical predictions ahead of experiments

https://doi.org/10.1515/pac-2025-0455
Received March 7, 2025; accepted May 6, 2025; published online May 26, 2025

Abstract: For decades, computational theoretical chemistry has provided critical insights into molecular behavior, often anticipating experimental discoveries. This review surveys twenty notable examples from the past fifteen years in which computational chemistry successfully predicted molecular structures, reaction mechanisms, and material properties before experimental confirmation. By spanning fields such as bioinorganic chemistry, materials science, catalysis, and quantum transport, these case studies illustrate how quantum chemical methods have become essential for multidisciplinary molecular sciences. The impact of theoretical predictions across disciplines shows the indispensable role of computational chemistry in guiding experiments and driving scientific discovery.

Keywords: computational chemistry; molecular design and discovery; multidisciplinary research; quantum chemical predictions; quantum science and technology; theoretical versus experimental chemistry.

Introduction

The United Nations has designated 2025 as the International Year of Quantum Science and Technology (IYQ). I am honored to have been invited to contribute to a special issue of *Pure and Applied Chemistry* that celebrates the role of quantum science and technology in computational theoretical chemistry during the IYQ. However, discussing such "impact" feels somewhat odd, as the field itself would not exist without the foundational principles of quantum mechanics.

Computational theoretical chemistry is the subfield of chemistry that simulates chemical processes through computational algorithms. Such algorithms directly translate the quantum laws into computer programs that predict molecular and supramolecular properties. Therefore, computational chemistry only makes sense in the context of the quantum mechanical description of molecular systems.

As Dirac noted in 1929, "The underlying physical laws necessary for the mathematical theory of a large part of physics and the whole of chemistry are thus completely known, and the difficulty is only that the exact application of these laws leads to equations much too complicated to be soluble."[1] Thanks to the entangled development of digital technologies and quantum chemical methodologies (Fig. 1), our approaches hold little similarity to those Dirac had access to at that time. But his assessment is still essentially correct. We still face significant challenges in solving many-body wave functions for fermionic systems, which typically require classical, statistical, or numerical approximations that inevitably degrade the accuracy of our predictions.

Article note: A collection of invited papers to celebrate the UN's proclamation of 2025 as the International Year of Quantum Science and Technology.

***Corresponding author: Mario Barbatti**, Aix Marseille University, CNRS, ICR, 13397 Marseille, France; and Institut Universitaire de France, 75231 Paris, France, e-mail: mario.barbatti@univ-amu.fr. https://orcid.org/0000-0001-9336-6607

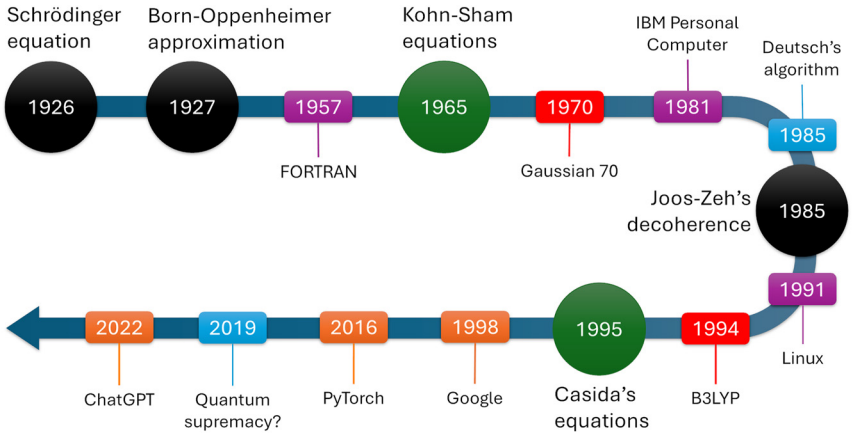

Fig. 1: Milestones in the development of theoretical chemistry (green circles) and its computational algorithmic and software expressions (red boxes) in a timeline with the key quantum mechanical developments for the field (black circles) and computational science infrastructure achievements (purple boxes). A profound reshaping of the field is occurring due to data science advances (orange boxes). It's still unclear, but future advances can emerge from quantum computing (blue boxes). For the scientific milestones, the dates correspond to the following references: Schrödinger equation (Ref. 2), Born-Oppenheimer approximation (Refs. 3,4), Kohn-Sham DFT equations (Ref. 5), Deutsch's algorithm (Ref. 6), Joos-Zeh's decoherence (Ref. 7), B3LYP functional (Ref. 8), and Casida's TDDFT equations (Ref. 9).

All these approximations leave us in constant tension between autonomous predictions and the need for experimental validation. I would not go as far as Lakatos and require that computational theoretical chemistry only be considered a progressive research program if it can predict novel empirical facts and at least some novel facts could be tested.[10] I recognize the value of our field by how much meaningful insight it brings to chemistry, even if its predictions come after the experiments. The chemistry community recognizes this value, too, as the field has been awarded at the highest level with the Nobel of Chemistry in 1998, 2013, and 2024. However, it's enormously satisfying when we can tap into the power of quantum mechanics of molecules and be experimentally corroborated afterward.

Therefore, the question I had in mind is how predictive computational theoretical chemistry is. I asked this question on X/Twitter in August 2024. (This happened before many scientists, including myself, migrated to other healthier social networks, mostly Bluesky.) I've gotten tremendous feedback from colleagues, many proudly showing off how their theoretical research has been empirically corroborated. I collected the answers and curated them. This paper is the result of this exercise. It aims to survey several case studies where theoretical chemical predictions were later experimentally corroborated. It spans various subfields – from bioinorganic chemistry to antimatter physics – illustrating how insightful Dirac was when he mentioned the "whole of chemistry."

I limited my survey to the last fifteen years. I also did not include papers lacking experimental confirmation (not even my favorite, when Chaer Nascimento and I predicted that H_5^+ clusters made a significant fraction of dense interstellar clouds composition[11]). I mostly avoided joint theoretical/experimental publications where it was unclear how much information flowed between labs.

As a warning, this survey must not be taken as expressing any quantitative publication or field statistics. If nothing else, it expresses confirmation bias, as only successful cases are reported. As a counterexample, I could cite the theoretical predictions of cyclobutanone S_2 lifetime, which span three orders of magnitude depending on the theoretical approach employed (Fig. 2). Moreover, each section delivers a compact account of the case study in point, focusing on a couple of theoretical and experimental papers. However, science never happens as isolated accidents. Each such case has rich histories that deserve in-depth reviews on their own. Therefore, I strongly recommend that the reader backtrack the literature cited in the papers I mentioned to build a more complete picture of each field.

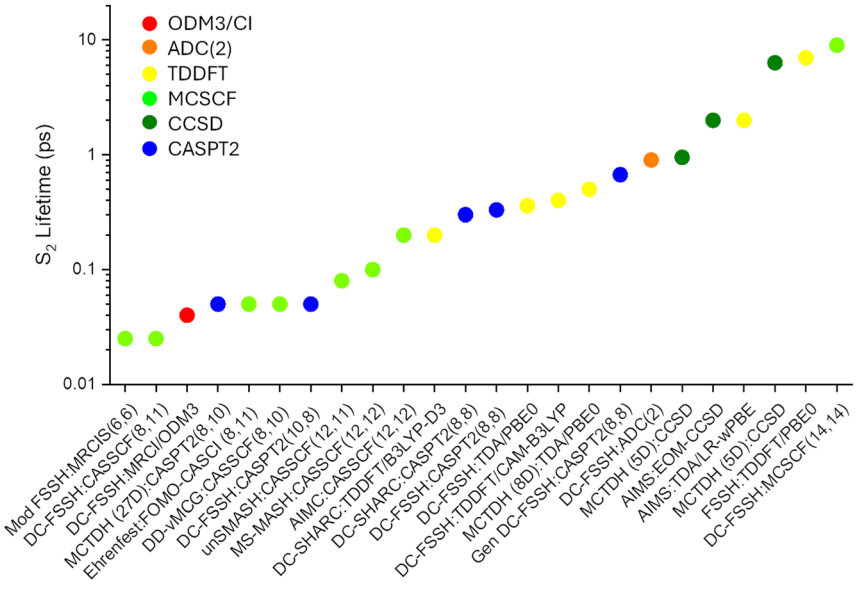

Fig. 2: S_2 excited-state lifetime of cyclobutanone predicted with different electronic structure and dynamics methods. Data from the papers published in the Journal of Chemical Physics special issue "Prediction Challenge: Cyclobutanone Photochemistry." See Ref. 12 and references therein for the data sources. Experimental results[13,14] were published after all simulations.

I mentioned how challenging it is to solve the quantum mechanics of molecules. This problem stems from the appalling sizes of the Hilbert space in many-body systems. Chemists, and not only theoretical ones, also face another challenge: the size of the chemical space, which means, the number of molecules that could exist. Until a decade ago, our only way to explore new molecules was through our chemical intuition aided by similarity and heuristics rules.

Recent developments in data science are reshaping the exploration of the chemical space, using machine learning to probe millions of different chemical species. Although it is a case of theory ahead of experiment, that's not a topic in this paper. I surveyed a couple of cases, but it would require a paper on its own to do a fair job, given the vast number of such works for material and catalyst designing.[15–19] More information on this topic can be found in these recent reviews.[20–23]

This paper is organized into two main sections. "Computational chemistry minimum" section reviews some key concepts and methods in computational theoretical chemistry, which will help non-specialist readers follow the case studies. "When theory came first: case studies" section surveys twenty studies where computational chemistry predictions were later experimentally confirmed.

Computational chemistry minimum

Computational theoretical chemistry predicts molecular properties using quantum mechanics. This section provides a brief overview of the main methods used in the case studies that follow in "When theory came first: case studies" section, focusing on the techniques applied there while acknowledging the existence of many other approaches.

Everything starts with the Schrödinger Equation for a molecular system

$$i\hbar \frac{\partial \Psi(\mathbf{R},\mathbf{r},t)}{\partial t} = \hat{H}\Psi(\mathbf{R},\mathbf{r},t) \tag{1}$$

where $\mathbf{R}$ represents the ensemble of nuclear coordinates, and $\mathbf{r}$ is the ensemble of electronic coordinates. Ψ is the molecular wave function and $\hat{H}$ the Hamiltonian operator. The enormous mass difference between nuclei and electrons allows us to invoke the Born-Oppenheimer approximation,[3] which decouples electronic and nuclear

subspaces. This decoupling yields an equation for the electrons (with energies E_n and wave function φ_n) at a fixed nuclear position:

$$\left(\hat{T}_{\text{elec}} + \hat{V}\right)\varphi_n = E_n\varphi_n \tag{2}$$

and an equation for the nuclei, with a wave function χ_n evolving on the potential energy surface (PES) E_n created by the electrons:

$$\left(\hat{T}_{\text{nuc}} + E_n\right)\chi_n = i\hbar\partial_t\chi_n \tag{3}$$

The Born-Oppenheimer approximation is the heart of molecular sciences. As expressed by Heller, it is "one of those wonderful approximations that even in failure forms the basis for discussion and systematic corrections."[24]

A lot of the everyday work of computational chemists is concerned with solving the electronic equation (2). A multitude of methods have been developed. Most adopt a bottom-up approach where one-electron wave functions (atomic orbitals) are combined to form molecular wave functions. The electronic wave function is still raw: the electrons do not know about each other. We must let them adapt and relax in the multielectron environment. We do that using electronic structure methods that recover such electronic correlation[25,26] so that Eq. (2) is satisfied (Fig. 3).

In most practical implementations, Eq. (2) is transformed into a nonlinear algebraic problem, typically solved iteratively using linear algebra techniques such as matrix construction, projection, and diagonalization steps within self-consistent or response-based frameworks.[28]

Among the electronic structure methods, Density Functional Theory (DFT) is the most widely used.[29] Instead of solving for the full N-electron wave function φ_n, DFT predicts the electronic density $\rho(\mathbf{r})$, reducing the problem to three spatial dimensions. This impressive dimensionality reduction is achieved by introducing functionals that curb the electronic energy to hold a specific dependence on $\rho(\mathbf{r})$. These functionals, ranging from simple expressions to complex parameterized forms, are imposed ad hoc, meaning DFT is not strictly an ab initio method.[30]

To describe excited electronic states, we use Time-Dependent Density Functional Theory (TDDFT).[31] It extends DFT to capture a molecule's response to time-dependent external fields, allowing the calculation of excitation energies and absorption spectra with a balance of accuracy and computational cost.

The efficiency of DFT and TDDFT makes them the workhorses of computational chemistry. Most of the cases I surveyed used DFT. "Computational discovery of dyes" and "Magnetic dipole transition moments in chiral helical molecules" sections apply TDDFT, too.

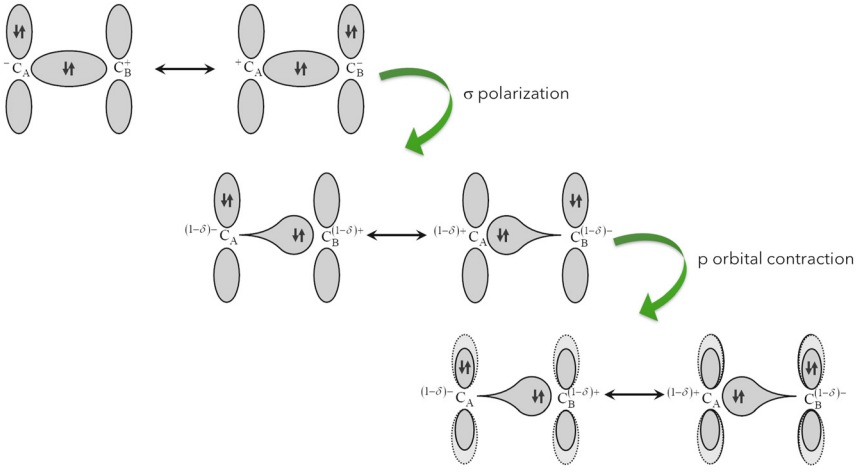

Fig. 3: Schematic illustration of electronic correlation recovered by electronic structure calculations for ethylene ππ* state, starting from a raw, single-configuration wave function composed of independent-electron orbitals. A significant part of electronic correlation corresponds to the orbitals' adaptation to the multielectronic environment; another part, not illustrated here, comes from adopting flexible, multi-configuration wave functions. See Ref. 27 for a discussion of the ethylene case and Ref. 25 for an analysis of electron correlation in a broader context.

For more accurate electronic excitation descriptions, particularly in materials and extended molecular systems, the GW approximation (named after the Green's function G and the screened Coulomb interaction W) and the Bethe-Salpeter Equation (BSE) provide powerful alternatives.[32] The GW method improves quasiparticle energy predictions by including electron-electron self-energy corrections, making it essential for computing electronic band structures. BSE, built upon GW, explicitly treats electron-hole interactions, yielding accurate optical excitation spectra. These methods are used in "Positronic bonding in molecular dianions" section.

Describing the electronic structure may require more involved methods when dealing with complex situations, such as dissociation, bond formation, multielectronic excited states, and conical intersections. Complete active space perturbation theory to the second order (CASPT2) is one of the primary choices in such cases.[33] It combines complex wave function initial guesses, advanced coefficient optimizations, and perturbative corrections to recover electron correlations. It is used in "Ultrafast heme-CO photolysis and spin-crossover in myoglobin" section.

Once we have electronic densities and energies, we look back to pick up all the effects left out in the long chain of approximations we used to solve the electronic problem. Then, computational chemists will work to recover relativistic effects, nonadiabatic couplings, and interactions with external fields.[34]

Next, we can focus on the nuclear problem, Eq. (3). However, even before attempting to solve this equation, we can learn much about nuclear distribution by mapping the PES topography. Their minima will reveal equilibrium structures, and their maxima will tell us about transition states. Much of computational chemistry focuses on finding pathways on those surfaces to describe chemical reactions.[35]

The quest to solve the nuclear equation starts by realizing that near the minima, PES are nearly multidimensional parabolas. The parabolic shape allows us to analyze the vibrational nuclear motion in terms of a collection of normal (in the sense of orthogonal) harmonic modes.

The relative simplicity of the ground state PES near the minima even allows us to fit the atomic interactions with simple functions.[36] It yields force fields, which are then used for molecular mechanics (MM), replacing the quantum nuclear distribution with classical nuclear motions obtained from molecular dynamics (MD). Force fields are employed in "Molecular insights into supramolecular polymer dynamics", "Predicting peptide self-assembly through computational discovery", "Computational insights into DNA methyltransferase neomorphism", and "Computational screening of enantioselective catalysts" sections. Force fields will not work if chemical bonds break (or form), electronic charges transfer between nuclei, or the molecule is electronically excited. In such cases, MD simulations on quantum-derived PES provide a more accurate treatment of nuclear motion.[37]

When quantum effects play too big of a role, we must step up our treatment of Eq. (3), which must be reformulated beyond the Born-Oppenheimer approximation to account for multiple states and their couplings.[38] Often, the time evolution of the nuclear wave function χ_n can be represented by ensembles of mixed quantum–classical trajectories.[39] Nevertheless, if nuclear delocalization or wave-like behavior is dominant (like in tunneling, for instance), wavepacket-based approaches,[40] such as the Multiconfigurational Time-Dependent Hartree (MCTDH) method, are required, as used in "Ultrafast heme-CO photolysis and spin-crossover in myoglobin" section.

In case interactions with the environment become too significant, such as in charge transport or quantum dissipation, different approaches are required for treating nuclear and electronic dynamics. For nuclear motion in dissipative systems, the reduced density matrix evolving according to a master equation[41] provides a framework for decoherence and energy relaxation (see "Shear-induced nucleation in molecular crystallization" and "Chirality-induced spin selectivity in electron transfer reactions" sections). One of the most advanced methods in this category is the Hierarchical Equations of Motion (HEOM) approach,[42] used in "Chirality-induced spin selectivity in electron transfer reactions" section. In turn, for electronic transport in molecular junctions and nanoscale devices, the Nonequilibrium Green's Function (NEGF) formalism[43] provides an excellent option, particularly in molecular electronics. It is used in "Increasing conductance in cumulene wires" section.

When theory came first: case studies

Bioinorganic chemistry

Revising the oxidation state of an iron–oxygen complex

The oxidation state of iron in transition metal-oxygen species is critical for bioinorganic chemistry and catalysis, including its role in photosystem II. In 2010, Fukuzumi and co-workers[44] reported a Fe–O complex capped by a Sc^{3+} ligand, assigning a Fe(IV) oxidation state based on crystallographic data. However, this interpretation was later challenged by theoretical and experimental studies.

Swart employed DFT calculations to analyze the structural and electronic properties of the Sc^{3+}-capped iron–oxygen species.[45] His results indicated that the Fe–O bond length (1.75 Å) was inconsistent with Fe(IV), instead corresponding to a high-spin Fe(III) center, with a water ligand rather than hydroxide coordinated to scandium. The computational analysis provided a strong argument for revising the oxidation state assignment.

Experimental confirmation followed when Prakash et al.[46] synthesized and characterized the complex using Mössbauer spectroscopy, electron paramagnetic resonance (EPR), and X-ray absorption spectroscopy. Their results unambiguously established that the iron center was in a high-spin Fe(III) state, not Fe(IV), aligning with Swart's theoretical prediction. The study also demonstrated that only one equivalent of ferrocene was needed to reduce the complex to Fe(II), further supporting the Fe(III) assignment. Because of the finding of a Fe(III) oxidation state, Zhou and co-workers then moved one step further and synthesized the Fe(III)-O-Cr(III) species to allow further spectroscopic characterization.[47]

Materials science

Computational discovery of dyes

Optimizing donor–π–acceptor (D–π–A) dyes is a central goal in improving dye-sensitized solar cells (DSCs). However, as I discussed in the Introduction, we only started to have the tools to search large regions of the chemical space with recent developments in data science techniques. The work discussed in this section is such an example.

Santaloci et al.[17] applied an automated quantum chemistry approach to design novel D–π–A dyes tailored for efficient near-infrared (NIR) absorption. The study began with a large-scale computational screening of 7,906 theoretically derived molecular dyes constructed by systematically combining various donor, bridge, and acceptor moieties. DFT and TDDFT calculations were used to optimize molecular geometries, compute absorption spectra, and assess electronic properties (Fig. 4-top).

This computational screening resulted in the identification of a promising dye, WM3 (Fig. 4-bottom), which was predicted to exhibit superior power conversion efficiency (PCE). The researchers then synthesized and characterized this dye. As expected, WM3 demonstrated strong NIR absorption, with an absorption onset at 760 nm and a PCE of 17.5 %, closely matching the theoretical predictions.

Shear-induced nucleation in molecular crystallization

Crystallization is traditionally understood through classical nucleation theories, emphasizing temperature and supersaturation as dominant factors. However, the work I review in this section has suggested that shear flow may play a nontrivial role in nucleation mechanisms, challenging those conventional models.

Mura and Zaccone[48] developed a theoretical framework combining the Becker-Doering master equation, the Smoluchowski diffusion-advection equation, and Kramers' escape rate theory to model the competition between

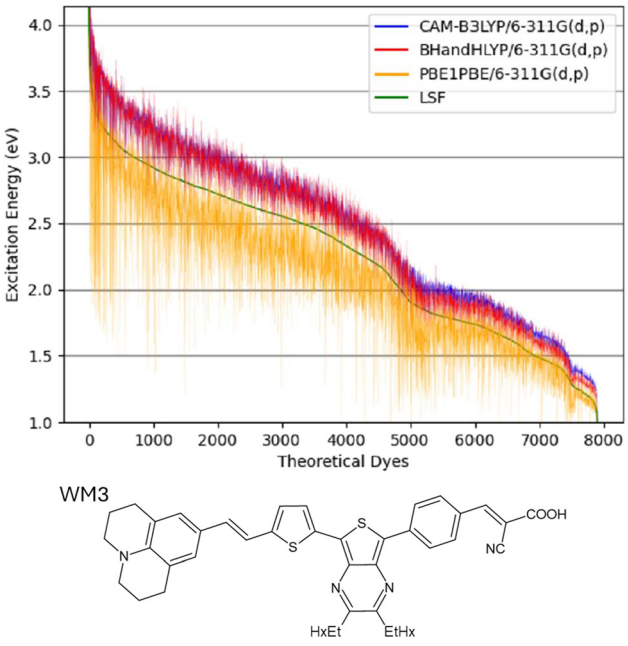

Fig. 4: (Top) Excitation energy distribution of 7,906 screened D–π–A dyes, computed with different DFT functionals. The LSF curve (green) highlights the trend toward NIR absorption. (Bottom) Structure of the selected dye (WM3), validated for high DSC performance. Adapted from Ref. 17.

shear-enhanced transport and mechanical straining of nuclei. Their simulations showed that nucleation rates exhibit a nonmonotonic dependence on shear rate.

Debuysschère et al.[49] tested Mura and Zaccone's prediction by studying glycine crystallization under shear conditions. Their experiments confirmed that nucleation rates increase with shear due to enhanced mass transport and nucleus coalescence. On the other hand, they also observed that the rates decrease at high shear due to mechanical deformation of nuclei. Using a microfluidic crystallization setup, they observed a strong correlation between their data and theoretical models, supporting the role of intermediate aggregation structures in a nonclassical nucleation pathway.

Localized antiaromaticity-driven cyclization in helicenes

The structural and electronic properties of helicenes make them unique platforms for studying charge delocalization and aromaticity effects. A significant prediction was made by Zhou et al.,[50] who computationally demonstrated that negative charge localization could drive a novel reductive cyclization mechanism in bis- and mono-helicenes. Based on DFT calculations, their study revealed that introducing a pentagonal unit into a helicene framework creates an antiaromatic hotspot, which drives a sequence of ring closures, leading to new graphene subunits.[51]

Deprotonation creates a localized antiaromatic region, selectively guiding electron addition. Nucleus-independent chemical shift (NICS) calculations using the gauge-including atomic orbitals (GIAO) method confirmed this effect by providing quantitative evidence of localized antiaromaticity. Meanwhile, molecular electrostatic potential (MEP) maps revealed the role of charge localization in dictating regioselectivity. Ultimately, the suppression of antiaromaticity emerged as the key factor facilitating the cyclization reaction. Frontier molecular orbital (FMO) analysis further supported the regioselective nature of the reaction. The theoretical findings indicated that the first cyclization step should occur at a site remote from the existing pentagonal unit rather than adjacent.

This counterintuitive prediction was later confirmed experimentally by interrupting the bis-annulation cascade through controlled exposure to molecular oxygen, allowing the isolation of the monoanionic intermediate. Its structure was unambiguously determined by X-ray crystallography, confirming that the first cyclization occurs at the remote site as predicted by theory.[51]

Supramolecular chemistry

Molecular insights into supramolecular polymer dynamics

Understanding the dynamics of supramolecular polymers is essential for designing materials with tunable properties, such as self-healing and adaptability. However, experimental characterization of monomer exchange in these systems has remained challenging due to spatial and temporal resolution limitations. The work I review here shows how computational chemistry has provided crucial insights into these processes, allowing the prediction of monomer exchange mechanisms ahead of experimental confirmation.

Bochicchio et al.[52] used all-atom and coarse-grained MD simulations to examine how monomers exchange in benzenetricarboxamide (BTA) supramolecular polymers. Their results indicate that exchange primarily occurs at defect sites along the polymer backbone rather than through a single-step process. Metadynamics simulations further revealed a two-step mechanism: monomers diffuse onto the fiber surface before detaching into the solvent. Notably, monomer incorporation and surface diffusion were significantly faster than desorption, revealing a kinetic asymmetry in the exchange process.

These theoretical predictions were later experimentally validated by Archontakis et al.[53] They used a super-resolution microscopy technique, which directly allowed the visualization of local defects and heterogeneities in supramolecular fibers. Their findings confirmed that monomer exchange predominantly occurs at structurally disordered domains, consistent with the computationally predicted exchange hotspots.

Predicting peptide self-assembly through computational discovery

The self-assembly of peptides into nanostructures is a key for nanotechnology, biomedicine, and materials science. Despite significant interest, predicting self-assembly behavior directly from peptide sequences has remained a major challenge. But that may be about to change, thanks to the advances in data science techniques.

Frederix et al.[54] addressed this self-assembly problem with computational theoretical chemistry. They systematically screened all 8,000 possible tripeptide sequences for their aggregation propensity in water. Using coarse-grained MD simulations, they developed an aggregation propensity score. They introduced a hydrophilicity-corrected version to prioritize peptides that balance self-assembly with water solubility. Their analysis revealed that aromatic residues such as phenylalanine, tyrosine, and tryptophan promote aggregation when placed in the second or third position, while positively charged or hydrogen-bonding residues at the N-terminus and negatively charged residues at the C-terminus enhance self-assembly.

In the same paper, Frederix and co-authors reported the synthesis and test of multiple tripeptides predicted by their computational modeling.[54] Those peptides that followed the design rules derived from simulations exhibiting hydrogel formation, representing the first example of unprotected tripeptides undergoing gelation at neutral pH. Spectroscopic and microscopic analyses confirmed the fibrous nanostructures, supporting the computational predictions.

Molecular electronics and quantum transport

Increasing conductance in cumulene wires

Understanding charge transport through molecular wires is crucial for developing molecular electronics. When tunneling is the dominant transport mechanism, the single-molecule conductance decreases exponentially with molecular length as the tunneling barrier width increases.

The possibility of reversing this exponential attenuation was first suggested in 2004 by Tada and Yoshizawa, who predicted increasing conductance with length in specific molecular systems.[55] Subsequent studies proposed various molecular wires exhibiting this behavior without invoking bond-length alternation (BLA).[56] The connection between BLA and conductance increasing emerged later as a theoretical curiosity[57] before being

formally investigated in specific molecular systems. Another key insight was that diradical character, rather than BLA alone, can also facilitate this conductance increase, as demonstrated in subsequent theoretical studies exploring various molecular candidates.[58]

However, no molecules that fulfill this condition had been found until Garner et al.[59] demonstrated, using DFT and NEGF calculations, that cumulenes – linear chains of sp-hybridized carbons with successive double bonds – exhibit reverse BLA, increasing electronic transmission with length (Fig. 5).

Their computational analysis showed that the dominant π-system has a reversed bond-length pattern for even-carbon cumulenes compared to polyynes or conjugated alkenes, resulting in a negative decay constant and meaning that conductance increases with length. They attributed the origin of this effect to the narrowing of the HOMO-LUMO gap with increasing length.

Zang et al.[60] later experimentally confirmed this effect using scanning tunneling microscope break-junction measurements. They synthesized and studied a series of cumulenes and polyynes ranging from 4 to 8 carbon atoms. These molecules were functionalized with thiomethyl groups to form junctions with gold electrodes. The measurements showed that while polyynes exhibited the expected exponential decay in conductance, cumulenes displayed the opposite trend, increasing their conductance with molecular length.

Spectroscopy

Anharmonicity and protonation in water clusters

As discussed in the Introduction, accuracy is a constant challenge for computational chemistry. Therefore, it is particularly satisfying when theory can tell experimentalists precisely where to look for phenomenological signatures. Such is the case in the study I review in this section. It deals with the behavior of excess protons in water, which is central to acid-base chemistry and proton transport.

The $H^+(H_2O)_{21}$ cluster, known for its exceptional stability, has been debated regarding whether its proton adopts an Eigen (H_3O^+) or Zundel ($H_5O_2^+$) structure. Torrent-Sucarrat and Anglada[61] applied vibrational second-order perturbation theory (VPT2) at a DFT level to model the infrared spectrum of $H^+(H_2O)_{21}$, including anharmonic effects. Their calculations indicated that the characteristic H_3O^+ stretches, typically observed near 2,500 cm^{-1}, undergo a substantial redshift of over 500 cm^{-1}, shifting below 2,000 cm^{-1}. This finding suggests that earlier studies, constrained to higher frequency ranges, may have overlooked crucial protonation signatures.

Fournier et al.[62] later explored this spectral window using cryogenic ion vibrational spectroscopy, detecting features around ~2,000 cm^{-1} that closely aligned with theoretical predictions, supporting the Eigen structure assignment over the Zundel alternative.

Interfacial water vibrations and their spectroscopic signature

Water's molecular structure and dynamics at interfaces play a crucial role in atmospheric chemistry and biological processes. Yet, despite extensive research, some vibrational modes at the air/water interface remain unidentified.

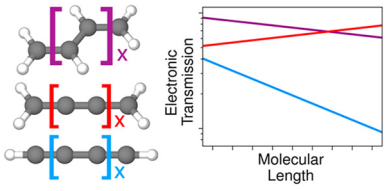

Fig. 5: Schematic comparison of bond-length alternation and electronic transmission trends in molecular wires. Left: Structural representations of different molecular systems, highlighting distinct bond-length alternation patterns. Right: Schematic representation of how electronic transmission changes with the molecular length for different bonding motifs, with cumulenes (red) exhibiting increasing conductance, polyynes (blue) showing conductance decay, and an intermediate system (purple) maintaining nearly constant transmission. Reprinted with permission from Ref. 59 Copyright 2018 American Chemical Society.

Perry et al.[63] used MD simulations with quantum-corrected time correlation functions and instantaneous normal mode analysis to predict a previously unknown vibrational mode at 875 cm^{-1}. They attributed it to the wagging motion of individual water molecules at the interface. In this mode, the water molecules are nearly parallel to the surface, with their hydrogen atoms oscillating perpendicular to the interface. Simulations of sum frequency generation (SFG) spectra using a point atomic polarizability approximation model indicated that this mode is a dominant structural feature alongside the well-established free OH vibrational signal.

These theoretical predictions were later validated by experimental SFG spectroscopy conducted by Tong et al.[64] They observed a librational mode of interfacial water at 834 cm^{-1}, with the same spectral lineshape, that is unique to the interface and qualitatively different than bulk librations. Their results confirmed that terminating the hydrogen-bond network at the air/water interface stiffens the rotational potential of water molecules.

Molecular magnetism and spintronics

Record high magnetic exchange in endohedral metallo-fullerenes

Understanding magnetic exchange interactions is critical for the design of single-molecule magnets (SMMs). Singh et al.[65] employed wave-function-based methods and DFT calculations to investigate the magnetic properties of $Ln_2@C_{79}N$ (Ln = Gd, Dy) molecules (Fig. 6), predicting record-high magnetic exchange interactions and a substantial barrier for magnetization reversal. Their computational results revealed an unprecedented ferromagnetic exchange interaction of approximately 200 cm^{-1} between the Gd(III) ions and the radical nitrogen-doped fullerene cage, an order of magnitude larger than previously reported radical–lanthanide interactions.[65]

For the anisotropic $Dy_2@C_{79}N$ system, calculations revealed that the strong Dy-radical exchange significantly suppresses quantum tunneling of magnetization (QTM), a key limitation in SMM performance. The computed magnetization blockade barrier exceeded 580 cm^{-1}, a value among the highest reported at the time. This enhancement arises from direct exchange coupling and charge transfer from the fullerene cage to the lanthanide ions.[65]

Subsequent experimental studies confirmed these predictions.[66] High-frequency electron paramagnetic resonance (HF-EPR) measurements on $Gd_2@C_{79}N$ established a ferromagnetic ground state with a total spin of $S = 15/2$, which agrees with theoretical predictions. The estimated exchange constant (~170 cm^{-1}) closely matched computational results. Additionally, magnetization studies on $Dy_2@C_{79}N$ demonstrated that the strong Dy-radical exchange effectively quenches QTM, leading to slow magnetization relaxation and a high blocking temperature.[67]

Chirality-induced spin selectivity in electron transfer reactions

Chirality-induced spin selectivity (CISS) has been widely studied in chiral molecules on surfaces.[68] Still, its role in free molecular electron transfer remained unclear. Fay and Limmer[69] predicted that CISS could arise in chiral donor-acceptor systems through spin–orbit coupling, electron hopping, and exchange interactions. Using

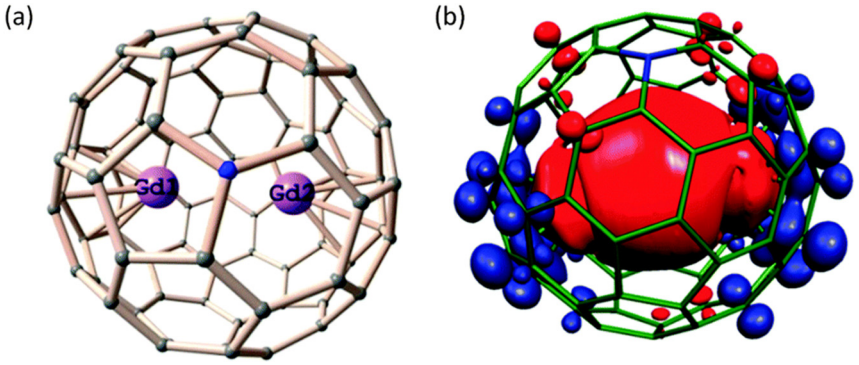

Fig. 6: (a) DFT optimized structure of the $Gd_2@665\text{-}(C_{79}N)$ isomer along with (b) its spin density plot for the $S = 15/2$ state. Reproduced from Ref. 65.

quantum master equations derived via the Nakajima-Zwanzig projection operator technique and validated with HEOM simulations, their model showed that spin polarization emerges dynamically (Fig. 7), displaying a non-monotonic temperature dependence independent of spin–orbit coupling strength.

These predictions were experimentally confirmed by Eckvahl et al.,[70] who used time-resolved electron paramagnetic resonance (EPR) to directly observe CISS in donor-acceptor molecules. Their results demonstrated that chiral bridges induce spin-polarized radical pairs, even in free molecules, without requiring an electrode interface, thereby establishing CISS as an intrinsic molecular property.

Magnetic dipole transition moments in chiral helical molecules

The magnetic dipole transition moment m is pivotal in chiroptical responses such as electronic circular dichroism and circularly polarized luminescence. However, strategies for systematically optimizing m have remained elusive, hindering the development of advanced optoelectronic and spintronic applications.

Uceda et al.[71] tackled this challenge by exploring the relationship between molecular structure and m values in three distinct families of fully π-conjugated helical molecules: carbo[n]helicenes, *ortho*-oligophenylethynylenes (o-OPEs), and chiral molecular circuits based on paracyclophanes. Using DFT and TDDFT calculations, they found that m values correlate linearly with the inner helical area of these molecules, akin to the behavior of classical solenoids.

Using unsupervised machine learning clustering,[18] the researchers identified specific electronic transitions where the magnetic dipole transition moment aligns with the helix axis. These transitions exhibited exceptional m values, reaching up to 47×10^{-20} erg G^{-1} in specific molecular circuits. This correlation provides a predictive tool for designing chiral molecules with enhanced chiroptical responses, which is relevant for applications in opto-electronics and spin-selective electrochemical processes.

Experimental validation confirmed these theoretical predictions:[18] the synthesis and X-ray characterization of 2,3,14,15-tetrabromo[6]helicene, followed by electronic circular dichroism (ECD) measurements, corroborated the model's prediction of its exceptional rotatory strength.

Coordination chemistry

Stabilization of neptunyl complexes with pyrrophen ligands

Understanding actinyl coordination is essential for actinide chemistry, particularly in nuclear waste management and separation processes. Jennifer G et al.[72] used DFT to predict that pyrrophen ligands could stabilize high-valent actinyl species via strong equatorial coordination. Their study suggested that neptunyl(VI) complexes would exhibit shorter Np=O bond lengths and enhanced ligand-field effects.

Ducilon et al.[73] later confirmed these predictions by synthesizing and characterizing two neptunyl-pyrrophen complexes (NpO_2L_1 and NpO_2L_2). Single-crystal X-ray diffraction revealed near-linear O=Np=O bond angles and Np=O bond lengths consistent with theoretical expectations. Raman spectroscopy further supported the presence of Np(VI). Their study also showed how ligand modifications influence complex stability. The

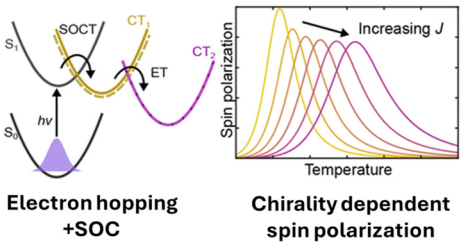

Fig. 7: Mechanism of chirality-induced spin polarization in electron transfer reactions. The left panel illustrates the role of spin–orbit coupling and electron hopping in charge transfer (CT) between molecular states, where intersystem crossing (SOCT) facilitates spin-mixing. The right panel shows the predicted temperature dependence of spin polarization, where increasing electronic exchange interaction (J) enhances spin selectivity, as modeled by quantum master equations. Adapted with permission from Ref. 69 Copyright 2021 American Chemical Society.

methyl-substituted ligand (L_2) resulted in slightly shorter Np=O bonds, indicating enhanced equatorial electron donation, as predicted computationally.

Physical organic chemistry

Heavy-atom tunneling in the cope rearrangement of semibullvalene

When we speak of quantum tunneling, we mainly associate it with light particles like electrons and protons. However, carbon tunneling may significantly affect organic reaction dynamics, at least at cryogenic temperatures, as I survey in this section.

Zhang et al.[74] employed theoretical methods to predict that the degenerate Cope rearrangement of semibullvalene could proceed rapidly at temperatures as low as 40 K due to carbon tunneling. Their DFT calculations of rate constants, including small-curvature tunneling corrections, suggested a rate constant of 1.43×10^{-3} s^{-1} at 40 K, leading to a half-life of approximately 8 min for the reaction (Fig. 8). Without tunneling, the process would be over ten orders of magnitude slower. The study proposed that an isotopically labeled semibullvalene could be a test case to experimentally confirm the effect.

Years later, Schleif et al.[75] experimentally validated this prediction using IR spectroscopy with matrix isolation techniques. They synthesized monodeuterated 1,5-dimethylsemibullvalene isotopomers and observed their rearrangement at 3 K. As predicted, the less stable isotopomer converted to the more stable one, even in the dark, with a rate constant of about 10^{-4} s^{-1}. Given the experimentally determined activation barrier of 4.8 kcal/mol, such a rate is too fast for classical thermal activation at these temperatures, thus confirming heavy-atom tunneling. The study further demonstrated that vibrational excitation via IR light could modulate the tunneling process, reinforcing the quantum mechanical nature of the reaction.

Triplet diradical carbocations: a new class of reactive intermediates

Carbocations have long been considered closed-shell singlet species. Yet, recent theoretical studies challenge this paradigm by predicting the existence of triplet diradical carbocations in specific molecular frameworks. A striking example of this is the work by Albright and Winter,[76] who used DFT calculations to demonstrate that donor-acceptor carbocations can stabilize open-shell configurations. Their computations indicated that certain

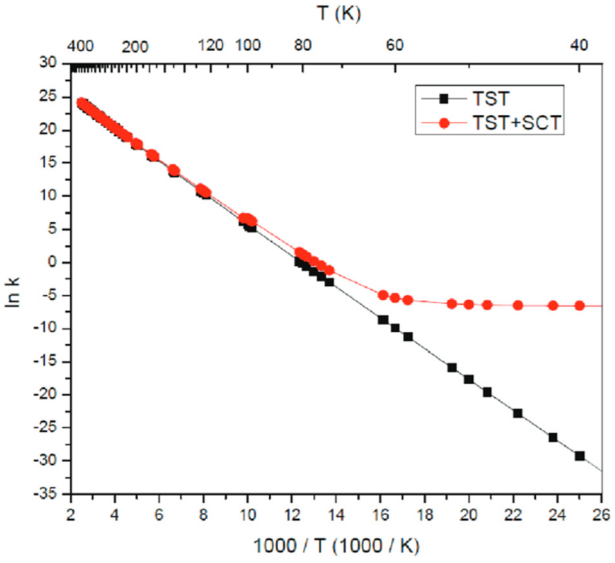

Fig. 8: Arrhenius plot of the rate constants computed with transition state theory (TST) and TST including small curvature tunneling (TST + SCT) for the Cope rearrangement of semibullvalene from 40 to 400 K. Reprinted with permission from Ref. 74 Copyright 2010 American Chemical Society.

coumarin and xanthenyl cations favor a triplet diradical ground state over a closed-shell singlet when substituted with strong electron-donating groups.

This theoretical prediction found experimental confirmation through spectroscopic studies on photolabile protecting groups, such as 7-diethylamino-4-methyl coumarin (DEACM) derivatives. In particular, Takano and Abe[77] reported the first direct experimental detection of a triplet diradical carbocation intermediate, confirming that the photoreaction of DEACM-Br involves the generation of a radical pair as well as a triplet carbocation intermediate. Their findings, supported by transient absorption spectroscopy and EPR measurements, provided compelling evidence that these carbocations exhibit diradical character in the triplet state.

Further supporting this concept, Nguyen and Abe[78] extended the study to (coumarin-4-yl)methyl derivatives with different leaving groups, revealing that the nature of these groups plays a crucial role in determining whether the reaction proceeds through a radical pair or an open-shell cationic intermediate. Their isotope-labeling experiments and quantum chemical calculations showed that, in some cases, the cation prefers an open-shell triplet ground state, preventing recombination with its counterion due to spin selection rules.

Ultrafast heme-CO photolysis and spin-crossover in myoglobin

The photolysis of carbon monoxide from myoglobin and the associated spin-crossover (SCO) transition of iron(II) plays a fundamental role in ligand dissociation and protein conformational changes. The microscopic mechanism of these reactions remained unclear due to the interplay between electronic and nuclear motions occurring on the femtosecond timescale.

In a project led by Huix-Rotllant, my colleague at the theoretical chemistry team in Marseille, Falahati and co-authors[79] employed quantum wavepacket dynamics using the Multi-Layer MCTDH method with a high-dimensional vibronic Hamiltonian fitted to CASPT2 data to elucidate this process. Their model incorporated 179 electronic states spanning singlet, triplet, and quintet manifolds, coupled to 15 vibrational modes, enabling the accurate description of nonadiabatic dynamics.

The simulations[79] revealed that upon photoexcitation, the Fe–CO bond undergoes coherent oscillations with a period of 42 fs and an amplitude of approximately 1 Å (Fig. 9). These nuclear motions drive irreversible CO dissociation and initiate sequential spin transitions, with the system relaxing into a triplet metal-to-ligand charge transfer (MLCT) state within ~75 fs and reaching the quintet state in ~430 fs. These computational findings demonstrated the crucial role of vibronic couplings in the ultrafast photodynamics of organometallic complexes.

Subsequent time-resolved serial femtosecond crystallography (TR-SFX) experiments by Barends et al.[80] confirmed these predictions. Under low fluence conditions, the expected oscillatory behavior of the Fe–CO bond was observed, just like in the simulations. However, a different dissociation mechanism emerged at higher fluences due to sequential two-photon absorption, bypassing the coherent oscillations and altering the spin-crossover dynamics.

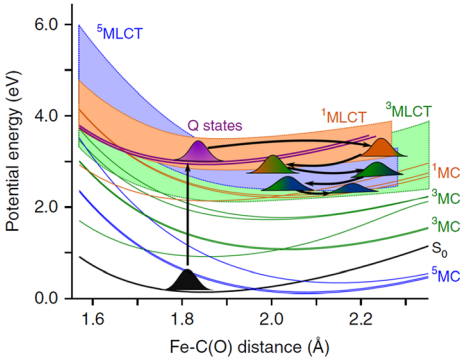

Fig. 9: Potential energy curves along the Fe–C(O) bond distance in myoglobin, computed using CASPT2. The initial photoexcitation (black arrow) populates the singlet metal-to-ligand charge transfer (^{1}MLCT) state, which undergoes vibronic coupling and nonadiabatic transitions. Wavepacket distributions illustrate the sequential population transfer from ^{1}MLCT to ^{3}MLCT, followed by transitions to metal-centered (MC) states and the eventual population of the quintet state (^{5}MC). The Q states (purple) mediate transitions between MLCT and MC states, governing the spin crossover and CO dissociation dynamics. Reproduced from Ref. 79.

Biochemical enzyme engineering

Computational insights into DNA methyltransferase neomorphism

Computational chemistry has proven instrumental in predicting enzymatic function, as demonstrated in the case of wild-type M.MpeI, a DNA methyltransferase with a neomorphic capability. Loo et al.[81] employed MD simulations with the AMBER force field to investigate the ability of an N374K mutant to utilize carboxy-S-adenosyl-L-methionine (CxSAM) instead of its native substrate, S-adenosyl-L-methionine (SAM). Energy decomposition analysis (EDA) was used to assess nonbonded interactions, revealing that the lysine substitution at position 374 introduces a favorable electrostatic interaction with the negatively charged carboxylate moiety of CxSAM, stabilizing its binding. Further modeling using root mean square fluctuation (RMSF), correlation matrices, and active site cavity volume calculations (CASTp 3.0) suggested that residue E45 plays a critical role in substrate discrimination, with the E45D mutation predicted to enhance selectivity for CxSAM (Fig. 10).

Experimental assays confirmed these predictions.[82] The N374K mutant exhibited methyltransferase and carboxymethyltransferase activities, while the E45D mutation alone did not affect CxSAM selectivity. However, when combined with N374K, the E45D mutation led to a pronounced preference for CxSAM over SAM. A direct competition assay further demonstrated this effect: while N374K retained SAM selectivity similar to the wild-type, the E45D/N374K variant reversed this preference. The findings have broad implications for biotechnology and epigenetic research, particularly in the selective modification of DNA.

Catalysis

Computational screening of enantioselective catalysts

The design of enantioselective catalysts is a critical challenge in asymmetric synthesis, impacting fields such as drug development and fine chemicals production. Computational chemistry has long been used to rationalize and predict stereoselectivity. Still, computational cost and methodological complexity have limited its application in large-scale catalyst screening. The path forward may be in the fruitful convergence of computational chemistry and data sciences.

Rosales et al.[83] introduced CatVS, an automated virtual screening tool based on quantum-guided MM, to efficiently predict stereoselectivity in asymmetric catalysis within hours. The method integrates transition state

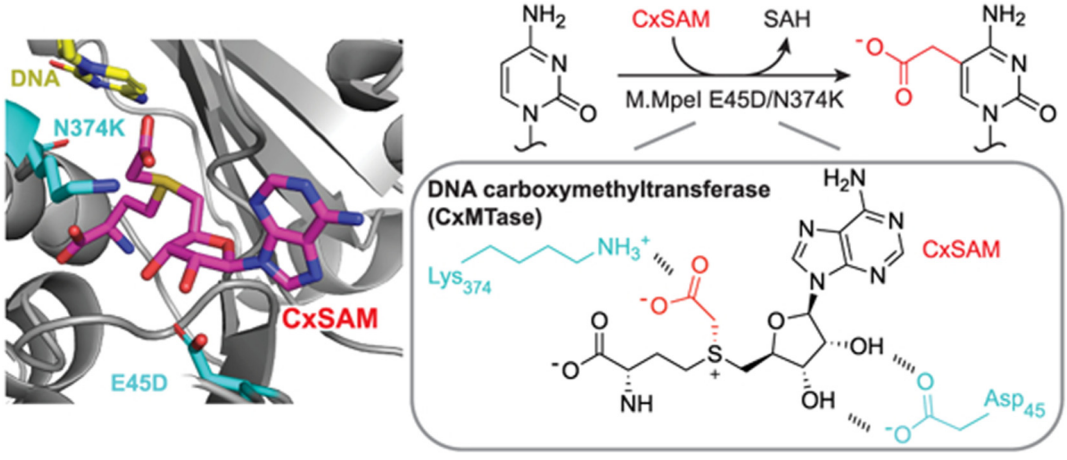

Fig. 10: Structural and mechanistic insights into M.MpeI E45D/N374K activity. Left: Active site representation showing key N374K and E45D interactions with CxSAM. Right: Schematic of the CxMTase reaction, highlighting the role of Lys374 and Asp45 in substrate recognition and catalysis. Reprinted (adapted) with permission from Ref. 81 Copyright 2023 American Chemical Society.

force fields derived from DFT calculations for efficient conformational sampling. Automated Monte Carlo and Low Mode searches further refine the transition states. This work builds on Norrby and co-authors' developments in quantum-guided molecular mechanics over two decades, consistently providing accurate enantioselectivity predictions without prior fitting to experimental data.[83,84] The automation introduced in CatVS allowed these predictions to be made before running experiments rather than as a post hoc validation, marking a shift in workflow rather than accuracy.

CatVS was applied to two well-known reactions to validate the method: the OsO_4-catalyzed *cis*-Dihydroxylation and the Rh-catalyzed asymmetric hydrogenation of enamides.[83] In the former, computational predictions closely matched experimental stereoselectivities, demonstrating the accuracy of the automated setup. In the latter, CatVS was used to screen a library of diphosphine ligands, successfully identifying the most selective candidates. Subsequent experimental testing confirmed the accuracy of the predictions, with four out of five ligands predicted to give high enantiomeric excesses (>98:2 e.r.) validated in the laboratory. While this approach remains highly predictive, specific systems present more significant deviations, which Rosales and co-authors analyzed in Ref. 85.

Computationally designed catalysts for the Morita–Baylis–Hillman reaction

Catalyst discovery is a cornerstone of modern synthetic chemistry, yet it has historically relied on intuition and trial-and-error experimentation. However, as I demonstrated in several earlier cases, data-driven approaches are revolutionizing this process. The following example further illustrates how such methodologies are reshaping catalyst design.

In a recent study, Seumer et al.[16] applied computational techniques to accelerate this process, using a genetic algorithm (GA) to explore chemical space in search of novel catalysts for the Morita–Baylis–Hillman (MBH) reaction. This reaction, catalyzed by tertiary amines, is widely used in organic synthesis, but improving its efficiency remains an open challenge.

The computational approach began with randomly selected tertiary amines, optimizing their structures for catalytic efficiency by iteratively evolving candidate molecules based on their predicted activation barriers. These barriers were estimated using GFN2-xTB (a semiempirical method increasingly employed for high-throughput screening[86–88]), allowing for rapid screening of many candidates. The GA identified 435 potential catalysts, with an overwhelming majority containing azetidine nitrogen as the active site. Notably, azetidines had not been previously reported as catalysts for the MBH reaction. Among the candidates, two molecules were chosen based on their synthetic accessibility and their predicted lower reaction barriers compared to the established catalyst DABCO. The most promising candidates were further refined using DFT calculations to compute complete reaction profiles and confirm the accuracy of the initial predictions.

Experimental validation confirmed the computational predictions.[16] One of the suggested azetidine catalysts was successfully synthesized and demonstrated an eightfold increase in catalytic activity over DABCO. The results validated the computational methodology and provided the first *de novo* discovery of an efficient catalyst using a generative algorithm.

Antimatter physics

Positronic bonding in molecular dianions

Positronic bonding offers a novel mechanism for stabilizing otherwise repulsive dianionic systems. Cassidy et al.[89] used many-body theory, a framework that accounts for complex electron-positron interactions beyond mean-field approximations, to predict the stability of positronically bonded molecular dianions of the form $[A^-; e^+; A^-]$, where A^- includes H^-, F^-, Cl^-, $(CN)^-$, and $(NCO)^-$. Their calculations, solving the Dyson equation for the

positron in the field of two anions, incorporated electron-positron correlations, including polarization, screening, and virtual-positronium formation. They employed the GW approximation for electron screening, BSE for electron-hole interactions, and ladder diagrams for positron-electron attraction. These methods revealed stable bonding configurations with bond energies around 1 eV and bond lengths of several ångströms. For [H^-; e^+; H^-], they confirmed a local minimum at ~3.4 Å, while at shorter separations ($r \lesssim 1.6$ Å), the system dissociates into H_2 and Ps^-. Their study extends prior theoretical work on positronic bonding in atomic anions, demonstrating its feasibility in molecular dianions like $(CN)_2^{2-}$ and $(NCO)_2^{2-}$.

Recent experimental work by Arthur-Baidoo et al.[90] on positron binding and annihilation in aromatic molecules supports the role of electron-positron correlations in determining binding energies. Their results show excellent agreement with the many-body theory, reinforcing its predictive accuracy.

Conclusions

Computational theoretical chemistry is remarkably flexible, as the case studies I selected for this review tell. From bioinorganic chemistry to quantum transport and antimatter studies, they illustrate how theoretical predictions may precede empirical discoveries and guide experimental design and interpretation. These success stories portray quantum chemical methods as tools enabling multidisciplinary research to explore the most diverse phenomena despite the inherent challenges of solving many-body quantum mechanical problems.

As computational techniques continue to evolve, particularly with the integration of artificial intelligence algorithms, the predictive capability of theoretical chemistry should expand even further. The dialog with experimentalists will always remain essential. However, the sizable number of cases where theory comes first reaffirms the fundamental role of quantum mechanics in chemistry and the ability of computational approaches to shape the future of molecular sciences.

My advice for young computational theoretical chemists is always to strive to make predictions. The ability to anticipate new molecular phenomena, reaction mechanisms, or material properties not only advances scientific knowledge but also strengthens the role of theoretical chemistry as a driving force for discovery. Even when predictions are later revised or refined, they provide valuable insights and challenge experimentalists to explore new possibilities. The most impactful theoretical work often arises from the courage to venture beyond known experimental data and propose something new.

Acknowledgments: I'm thankful to W. T. Borden, G. A. Cisneros, J. M. Cuerva, D. Dave, T. P. Fay, R. C. Fortenberry, I. Funes-Ardoiz, M. H. Garner, A. Gorden, D. G. Green, M. Huix-Rotllant, J. H. Jensen, C. Laconsay, P.-O. Norrby, G. M. Pavan, R. Poranne, R. Ramakrishnan, R. Rana, T. Santaloci, G. C. Solomon, B. Space, T. Stuyver, M. Swart, J. M. Toldo, M. Torrent-Sucarrat, R. G. Uceda, A. H. Winter, and A. Zaccone, who gave feedback on the manuscript and pointed me out to many relevant works for this review.
Research ethics: Not applicable.
Informed consent: Not applicable.
Author contributions: The author has accepted responsibility for the entire content of this manuscript and approved its submission.
Use of Large Language Models, AI and Machine Learning Tools: None declared.
Conflict of interest: The author states no conflict of interest.
Research funding: This work received support from the French government under the France 2030 investment plan as part of the Initiative d'Excellence d'Aix-Marseille Université (A*MIDEX AMX-22-REAB-173 and AMX-22-IN1-48) and from the European Research Council (ERC) Advanced Grant SubNano (grant agreement 832237).
Data availability: Not applicable.

References

1. Dirac, P. A. M.; Fowler, R. H. Quantum Mechanics of Many-Electron Systems. *Proc. R. Soc. London.-Ser. A Contain. Pap. Math. Phys. Character* 1997, *123*, 714–733. https://doi.org/10.1098/rspa.1929.0094
2. Schrödinger, E. An Undulatory Theory of the Mechanics of Atoms and Molecules. *Phys. Rev.* **1926**, *28*, 1049–1070. https://doi.org/10.1103/PhysRev.28.1049.
3. Born, M.; Oppenheimer, R. On the Quantum Theory of Molecules. In *Quantum Chemistry*; World Scientific: Singapore, Vol. 8, 2000; pp 1–24.
4. Born, M.; Oppenheimer, R. Zur Quantentheorie der Molekeln. *Ann. Phys.* **1927**, *389*, 457–484. https://doi.org/10.1002/andp.19273892002.
5. Kohn, W.; Sham, L. J. Self-Consistent Equations Including Exchange and Correlation Effects. *Phys. Rev.* **1965**, *140*, A1133–A1138. https://doi.org/10.1103/PhysRev.140.A1133.
6. Deutsch, D. Quantum Theory, the Church–Turing Principle and the Universal Quantum Computer. *Proc. R. Soc. London, A* **1985**, *400*, 97–117. https://doi.org/10.1098/rspa.1985.0070.
7. Joos, E.; Zeh, H. D. The Emergence of Classical Properties through Interaction with the Environment. *Z. Phys. B* **1985**, *59*, 223–243. https://doi.org/10.1007/bf01725541.
8. Stephens, P. J.; Devlin, F. J.; Chabalowski, C. F.; Frisch, M. J. Ab Initio Calculation of Vibrational Absorption and Circular Dichroism Spectra Using Density Functional Force Fields. *J. Phys. Chem.* **1994**, *98*, 11623–11627. https://doi.org/10.1021/j100096a001.
9. Casida, M. E., Time-Dependent Density Functional Response Theory for Molecules. In *Recent Advances in Density Functional Methods*; Chong, D. P., Ed. World Scientific: Singapore, Vol. 1, 1995; pp 155–192.
10. Lakatos, I., Falsification and the Methodology of Scientific Research Programmes. In *Criticism and the Growth of Knowledge: Proceedings of the International Colloquium in the Philosophy of Science, London, 1965*; Lakatos, I.; Musgrave, A., Eds. Cambridge University Press: Cambridge, 1970; Vol. *4*, pp 91–196.
11. Barbatti, M.; Nascimento, M. A. C. Does the H_5^+ Hydrogen Cluster Exist in Dense Interstellar Clouds? *Int. J. Quantum Chem.* **2012**, *112*, 3169–3173. https://doi.org/10.1002/qua.24110.
12. Mukherjee, S.; Mattos, R. S.; Toldo, J. M.; Lischka, H.; Barbatti, M. Prediction Challenge: Simulating Rydberg Photoexcited Cyclobutanone with Surface Hopping Dynamics based on Different Electronic Structure Methods. *J. Chem. Phys.* **2024**, *160*, 154306. https://doi.org/10.1063/5.0203636.
13. Green, A. E.; Liu, Y.; Allum, F.; Graßl, M.; Lenzen, P.; Ashfold, M. N. R.; Bhattacharyya, S.; Cheng, X.; Centurion, M.; Crane, S. W.; Forbes, R. G. ; Goff, N. A.; Huang, L.; Kaufman, B.; Kling, M. F.; Kramer, P. L.; Lam, H. V. S.; Larsen, K. A.; Lemons, R.; Lin, M. F.; Orr-Ewing, A. J.; Rolles, D.; Rudenko, A.; Saha, S. K.; Searles, J.; Shen, X.; Weathersby, S.; Weber, P. M.; Zhao, H.; Wolf, T. J. A. Imaging the Photochemistry of Cyclobutanone Using Ultrafast Electron Diffraction: Experimental Results. *arXiv [physics.chem-ph]* **2025**, *162*. https://doi.org/10.48550/arXiv.2502.13956.
14. Wang, T.; Jiang, H.; Jin, C.; Zou, X.; Zhu, P.; Jiang, T.; He, F.; Xiang, D. Imaging the Photochemical Dynamics of Cyclobutanone with MeV Ultrafast Electron Diffraction. *arXiv [physics.chem-ph]* **2025**, *162*. https://doi.org/10.48550/arXiv.2502.16236.
15. Hueffel, J. A.; Sperger, T.; Funes-Ardoiz, I.; Ward, J. S.; Rissanen, K.; Schoenebeck, F. Accelerated Dinuclear Palladium Catalyst Identification through Unsupervised Machine Learning. *Science* **2021**, *374*, 1134–1140. https://doi.org/10.1126/science.abj0999.
16. Seumer, J.; Kirschner Solberg Hansen, J.; Brøndsted Nielsen, M.; Jensen, J. H. Computational Evolution of New Catalysts For The Morita–Baylis–Hillman Reaction. *Angew. Chem. Int. Ed.* **2023**, *62*, e202218565. https://doi.org/10.1002/anie.202218565.
17. Santaloci, T. J.; Meador, W. E.; Wallace, A. M.; Valencia, E. M.; Rogers, B. N.; Delcamp, J. H.; Fortenberry, R. C. An Automated Quantum Chemistry-Driven, Experimental Characterization for High PCE Donor–π–Acceptor NIR Molecular Dyes. *Digit. Dicov.* **2023**, *2*, 1269–1288. https://doi.org/10.1039/D3DD00023K.
18. Uceda, R. G.; Gijón, A.; Míguez-Lago, S.; Cruz, C. M.; Blanco, V.; Fernández-Álvarez, F.; Álvarez de Cienfuegos, L.; Molina-Solana, M.; Gómez-Romero, J.; Miguel, D.; Mota, A. J.; Cuerva, J. M. Can Deep Learning Search for Exceptional Chiroptical Properties? The Halogenated [6]Helicene Case. *Angew. Chem. Int. Ed.* **2024**, *63*, e202409998. https://doi.org/10.1002/anie.202409998.
19. Korablyov, M.; Liu, C.-H.; Jain, M.; van der Sloot, A. M.; Jolicoeur, E.; Ruediger, E.; Nica, A. C.; Bengio, E.; Lapchevskyi, K.; St-Cyr, D.; Schuetz, D. A.; Butoi, V. I.; Rector-Brooks, J.; Blackburn, S.; Feng, L.; Nekoei, H.; Gottipati, S.; Vijayan, P.; Gupta, P.; Rampášek, L.; Avancha, S.; Bacon, P.-L.; Hamilton, W. L.; Paige, B.; Misra, S.; Jastrzebski, S. K.; Kaul, B.; Precup, D.; Hernández-Lobato, J. M.; Segler, M.; Bronstein, M.; Marinier, A.; Tyers, M.; Bengio, Y. Generative Active Learning for the Search of Small-Molecule Protein Binders. *arXiv [q-bio.BM]* **2024**. https://doi.org/10.48550/arXiv.2405.01616.
20. Lavecchia, A. Navigating the Frontier of Drug-Like Chemical Space with Cutting-Edge Generative AI Models. *Drug Discov. Today* **2024**, *29*, 104133. https://doi.org/10.1016/j.drudis.2024.104133.
21. Flores-Hernandez, H.; Martinez-Ledesma, E. A Systematic Review of Deep Learning Chemical Language Models in Recent Era. *J. Cheminf.* **2024**, *16*, 129. https://doi.org/10.1186/s13321-024-00916-y.
22. Mai, H.; Le, T. C.; Chen, D.; Winkler, D. A.; Caruso, R. A. Machine Learning for Electrocatalyst and Photocatalyst Design and Discovery. *Chem. Rev.* **2022**, *122*, 13478–13515. https://doi.org/10.1021/acs.chemrev.2c00061.
23. Shi, Y.-F.; Yang, Z.-X.; Ma, S.; Kang, P.-L.; Shang, C.; Hu, P.; Liu, Z.-P. Machine Learning for Chemistry: Basics and Applications. *Engineering* **2023**, *27*, 70–83. https://doi.org/10.1016/j.eng.2023.04.013.
24. Heller, E. J. *The Semiclassical Way to Dynamics and Spectroscopy*; Princeton University Press: Princeton, 2018.

25. Truhlar, D. G. Valence Bond Theory for Chemical Dynamics. *J. Comput. Chem.* **2007**, *28*, 73–86. https://doi.org/10.1002/jcc.20529.
26. Löwdin, P.-O. Correlation Problem in Many-Electron Quantum Mechanics I. Review of Different Approaches and Discussion of Some Current Ideas. *Adv. Chem. Phys.* **1958**, 207–322. https://doi.org/10.1002/9780470143483.ch7.
27. Angeli, C. On the Nature of the $\pi \rightarrow \pi^*$ Ionic Excited States: The V State of Ethene as a Prototype. *J. Comput. Chem.* **2009**, *30*, 1319–1333. https://doi.org/10.1002/Jcc.21155.
28. Helgaker, T.; Jørgensen, P.; Olsen, J. *Molecular Electronic-Structure Theory*; John Wiley & Sons: Chichester, 2000; pp 1–33.
29. Jones, R. O. Density Functional Theory: Its Origins, Rise to Prominence, and Future. *Rev. Mod. Phys.* **2015**, *87*, 897–923. https://doi.org/10.1103/RevModPhys.87.897.
30. Medvedev, M. G.; Bushmarinov, I. S.; Sun, J.; Perdew, J. P.; Lyssenko, K. A. Density Functional Theory Is Straying from the Path Toward the Exact Functional. *Science* **2017**, *355*, 49–52. https://doi.org/10.1126/science.aah5975.
31. Casida, M. E.; Huix-Rotllant, M. Progress in Time-Dependent Density-Functional Theory. *Annu. Rev. Phys. Chem.* **2012**, *63*, 287–323. https://doi.org/10.1146/annurev-physchem-032511-143803.
32. Golze, D.; Dvorak, M.; Rinke, P. The GW Compendium: A Practical Guide to Theoretical Photoemission Spectroscopy. *Front. Chem.* **2019**, *7*, 377. https://doi.org/10.3389/fchem.2019.00377.
33. Pulay, P. A Perspective on the CASPT2 Method. *Int. J. Quantum Chem.* **2011**, *111*, 3273–3279. https://doi.org/10.1002/qua.23052.
34. Liu, W. Perspective: Simultaneous Treatment of Relativity, Correlation, and QED. *WIREs: Comp. Mol. Sci.* **2023**, *13*, e1652. https://doi.org/10.1002/wcms.1652.
35. Dewyer, A. L.; Argüelles, A. J.; Zimmerman, P. M. Methods for Exploring Reaction Space in Molecular Systems. *WIREs: Comp. Mol. Sci.* **2018**, *8*, e1354. https://doi.org/10.1002/wcms.1354.
36. Groenhof, G., Introduction to QM/MM Simulations. In *Biomolecular Simulations: Methods and Protocols*; Monticelli, L.; Salonen, E., Eds.; Humana Press: Totowa, NJ, 2013; pp 43–66.
37. Sun, L.; Hase, W. L. Born–Oppenheimer Direct Dynamics Classical Trajectory Simulations. In *Reviews in Computational Chemistry*; Wiley-VCH: New York, 2003; pp 79–146.
38. Agostini, F.; Curchod, B. F. E. Different Flavors of Nonadiabatic Molecular Dynamics. *WIREs: Comp. Mol. Sci.* **2019**, *9*, e1417. https://doi.org/10.1002/wcms.1417.
39. Crespo-Otero, R.; Barbatti, M. Recent Advances and Perspectives on Nonadiabatic Mixed Quantum-Classical Dynamics. *Chem. Rev.* **2018**, *118*, 7026–7068. https://doi.org/10.1021/acs.chemrev.7b00577.
40. Worth, G. A.; Meyer, H. D.; Köppel, H.; Cederbaum, L. S.; Burghardt, I. Using the MCTDH Wavepacket Propagation Method to Describe Multimode Non-adiabatic Dynamics. *Int. Rev. Phys. Chem.* **2008**, *27*, 569–606. https://doi.org/10.1080/01442350802137656.
41. Manzano, D. A Short Introduction to the Lindblad Master Equation. *AIP Adv.* **2020**, *10*, 025106. https://doi.org/10.1063/1.5115323.
42. Kramer, T.; Noack, M.; Reinefeld, A.; Rodríguez, M.; Zelinskyy, Y. Efficient Calculation of Open Quantum System Dynamics and Time-Resolved Spectroscopy with Distributed Memory HEOM (DM-HEOM). *J. Comput. Chem.* **2018**, *39*, 1779–1794. https://doi.org/10.1002/jcc.25354.
43. Camsari, K. Y.; Chowdhury, S.; Datta, S., The Nonequilibrium Green Function (NEGF) Method. In *Springer Handbook of Semiconductor Devices*, Rudan, M.; Brunetti, R.; Reggiani, S., Eds.; Springer International Publishing: Cham, 2023; pp 1583–1599.
44. Fukuzumi, S.; Morimoto, Y.; Kotani, H.; Naumov, P.; Lee, Y.-M.; Nam, W. Crystal Structure of a Metal Ion-Bound Oxoiron(IV) Complex and Implications for Biological Electron Transfer. *Nat. Chem.* **2010**, *2*, 756–759. https://doi.org/10.1038/nchem.731.
45. Swart, M. A Change in the Oxidation State of Iron: Scandium Is Not Innocent. *Chem. Commun.* **2013**, *49*, 6650–6652. https://doi.org/10.1039/C3CC42200C.
46. Prakash, J.; Rohde, G. T.; Meier, K. K.; Jasniewski, A. J.; Van Heuvelen, K. M.; Münck, E.; Que, L. Jr. Spectroscopic Identification of an Fe^{III} Center, Not Fe^{IV}, in the Crystalline Sc–O–Fe Adduct Derived from $[Fe^{IV}(O)(TMC)]^{2+}$. *J. Am. Chem. Soc.* **2015**, *137*, 3478–3481. https://doi.org/10.1021/jacs.5b00535.
47. Zhou, A.; Kleespies, S. T.; Van Heuvelen, K. M.; Que, L. Characterization of a Heterobimetallic Nonheme Fe(iii)–O–Cr(iii) Species Formed by O_2 activation. *Chem. Commun.* **2015**, *51*, 14326–14329. https://doi.org/10.1039/C5CC05931C.
48. Mura, F.; Zaccone, A. Effects of Shear Flow on Phase Nucleation and Crystallization. *Phys. Rev. E* **2016**, *93*, 042803. https://doi.org/10.1103/PhysRevE.93.042803.
49. Debuysschère, R.; Rimez, B.; Zaccone, A.; Scheid, B. Experimental and Theoretical Investigation of Nonclassical Shear-Induced Nucleation Mechanism for Small Molecule. *Cryst. Growth Des.* **2023**, *23*, 4979–4989. https://doi.org/10.1021/acs.cgd.3c00232.
50. Zhou, Z.; Kawade, R. K.; Wei, Z.; Kuriakose, F.; Üngör, Ö.; Jo, M.; Shatruk, M.; Gershoni-Poranne, R.; Petrukhina, M. A.; Alabugin, I. V. Negative Charge as a Lens for Concentrating Antiaromaticity: Using a Pentagonal "Defect" and Helicene Strain for Cyclizations. *Angew. Chem. Int. Ed.* **2020**, *59*, 1256–1262. https://doi.org/10.1002/anie.201911319.
51. Zhou, Z.; Egger, D. T.; Hu, C.; Pennachio, M.; Wei, Z.; Kawade, R. K.; Üngör, Ö.; Gershoni-Poranne, R.; Petrukhina, M. A.; Alabugin, I. V. Localized Antiaromaticity Hotspot Drives Reductive Dehydrogenative Cyclizations in Bis- and Mono-Helicenes. *J. Am. Chem. Soc.* **2022**, *144*, 12321–12338. https://doi.org/10.1021/jacs.2c03681.
52. Bochicchio, D.; Salvalaglio, M.; Pavan, G. M. Into the Dynamics of a Supramolecular Polymer at Submolecular Resolution. *Nat. Commun.* **2017**, *8*, 147. https://doi.org/10.1038/s41467-017-00189-0.
53. Archontakis, E.; Dhiman, S.; Zhang, M.; Vleugels, M. E. J.; Meijer, E. W.; Palmans, A. R. A.; Zijlstra, P.; Albertazzi, L. Visualizing the Heterogeneity in Homogeneous Supramolecular Polymers. *J. Am. Chem. Soc.* **2024**, *146*, 19974–19985. https://doi.org/10.1021/jacs.4c03562.

54. Frederix, P. W. J. M.; Scott, G. G.; Abul-Haija, Y. M.; Kalafatovic, D.; Pappas, C. G.; Javid, N.; Hunt, N. T.; Ulijn, R. V.; Tuttle, T. Exploring the Sequence Space for (tri-)Peptide Self-assembly to Design and Discover New Hydrogels. *Nat. Chem.* **2015**, *7*, 30–37. https://doi.org/10.1038/nchem.2122.
55. Tada, T.; Yoshizawa, K. Reverse Exponential Decay of Electrical Transmission in Nanosized Graphite Sheets. *J. Phys. Chem. B* **2004**, *108*, 7565–7572. https://doi.org/10.1021/jp0310908.
56. Stuyver, T.; Fias, S.; De Proft, F.; Geerlings, P. The Relation Between Delocalization, Long Bond Order Structure Count and Transmission: An Application to Molecular Wires. *Chem. Phys. Lett.* **2015**, *630*, 51–56. https://doi.org/10.1016/j.cplett.2015.04.043.
57. Tsuji, Y.; Movassagh, R.; Datta, S.; Hoffmann, R. Exponential Attenuation of Through-Bond Transmission in a Polyene: Theory and Potential Realizations. *ACS Nano* **2015**, *9*, 11109–11120. https://doi.org/10.1021/acsnano.5b04615.
58. Stuyver, T.; Fias, S.; De Proft, F.; Geerlings, P.; Tsuji, Y.; Hoffmann, R. Enhancing the Conductivity of Molecular Electronic Devices. *J. Chem. Phys.* **2016**, *146*, 092310. https://doi.org/10.1063/1.4972992.
59. Garner, M. H.; Bro-Jørgensen, W.; Pedersen, P. D.; Solomon, G. C. Reverse Bond-Length Alternation in Cumulenes: Candidates for Increasing Electronic Transmission with Length. *J. Phys. Chem. C* **2018**, *122*, 26777–26789. https://doi.org/10.1021/acs.jpcc.8b05661.
60. Zang, Y.; Fu, T.; Zou, Q.; Ng, F.; Li, H.; Steigerwald, M. L.; Nuckolls, C.; Venkataraman, L. Cumulene Wires Display Increasing Conductance with Increasing Length. *Nano Lett.* **2020**, *20*, 8415–8419. https://doi.org/10.1021/acs.nanolett.0c03794.
61. Torrent-Sucarrat, M.; Anglada, J. M. Anharmonicity and the Eigen-Zundel Dilemma in the IR Spectrum of the Protonated 21 Water Cluster. *J. Chem. Theory Comput.* **2011**, *7*, 467–472. https://doi.org/10.1021/ct100692x.
62. Fournier, J. A.; Johnson, C. J.; Wolke, C. T.; Weddle, G. H.; Wolk, A. B.; Johnson, M. A. Vibrational Spectral Signature of the Proton Defect in the Three-Dimensional $H^+(H_2O)_{21}$ Cluster. *Science* **2014**, *344*, 1009–1012. https://doi.org/10.1126/science.1253788.
63. Perry, A.; Neipert, C.; Ridley, C.; Space, B.; Moore, P. B. Identification of a Wagging Vibrational Mode of Water Molecules at the Water/Vapor Interface. *Phys. Rev. E* **2005**, *71*, 050601. https://doi.org/10.1103/PhysRevE.71.050601.
64. Tong, Y.; Kampfrath, T.; Campen, R. K. Experimentally Probing the Libration of Interfacial Water: The Rotational Potential of Water Is Stiffer at the Air/Water Interface Than in Bulk Liquid. *Phys. Chem. Chem. Phys.* **2016**, *18*, 18424–18430. https://doi.org/10.1039/C6CP01004K.
65. Singh, M. K.; Yadav, N.; Rajaraman, G. Record High Magnetic Exchange and Magnetization Blockade in $Ln_2@C_{79}N$ (Ln = Gd(iii) and Dy(iii)) Molecules: A Theoretical Perspective. *Chem. Commun.* **2015**, *51*, 17732–17735. https://doi.org/10.1039/C5CC06642E.
66. Fu, W.; Zhang, J.; Fuhrer, T.; Champion, H.; Furukawa, K.; Kato, T.; Mahaney, J. E.; Burke, B. G.; Williams, K. A.; Walker, K.; Dixon, C.; Ge, J.; Shu, C.; Harich, K.; Dorn, H. C. Gd2@C79N: Isolation, Characterization, and Monoadduct Formation of a Very Stable Heterofullerene with a Magnetic Spin State of S = 15/2. *J. Am. Chem. Soc.* **2011**, *133*, 9741–9750. https://doi.org/10.1021/ja202011u.
67. Liu, F.; Krylov, D. S.; Spree, L.; Avdoshenko, S. M.; Samoylova, N. A.; Rosenkranz, M.; Kostanyan, A.; Greber, T.; Wolter, A. U. B.; Büchner, B.; Popov, A. A. Single Molecule Magnet with an Unpaired Electron Trapped between Two Lanthanide Ions Inside a Fullerene. *Nat. Commun.* **2017**, *8*, 16098. https://doi.org/10.1038/ncomms16098.
68. Naaman, R.; Waldeck, D. H. Chiral-Induced Spin Selectivity Effect. *J. Phys. Chem. Lett.* **2012**, *3*, 2178–2187. https://doi.org/10.1021/jz300793y.
69. Fay, T. P.; Limmer, D. T. Origin of Chirality Induced Spin Selectivity in Photoinduced Electron Transfer. *Nano Lett.* **2021**, *21*, 6696–6702. https://doi.org/10.1021/acs.nanolett.1c02370.
70. Eckvahl, H. J.; Tcyrulnikov, N. A.; Chiesa, A.; Bradley, J. M.; Young, R. M.; Carretta, S.; Krzyaniak, M. D.; Wasielewski, M. R. Direct Observation of Chirality-Induced Spin Selectivity in Electron Donor–Acceptor Molecules. *Science* **2023**, *382*, 197–201. https://doi.org/10.1126/science.adj5328.
71. Uceda, R. G.; Cruz, C. M.; Míguez-Lago, S.; de Cienfuegos, L. Á.; Longhi, G.; Pelta, D. A.; Novoa, P.; Mota, A. J.; Cuerva, J. M.; Miguel, D. Can Magnetic Dipole Transition Moment Be Engineered? *Angew. Chem. Int. Ed.* **2024**, *63*, e202316696. https://doi.org/10.1002/anie.202316696.
72. Jennifer, G, A.; Gao, Y.; Schreckenbach, G.; Varathan, E. Periodic Trends in the Stabilization of Actinyls in Their Higher Oxidation States Using Pyrrophen Ligands. *Inorg. Chem.* **2023**, *62*, 6920–6933. https://doi.org/10.1021/acs.inorgchem.3c00022.
73. Ducilon, J.; Nicholas, A. D.; Surbella, R. G.; Gorden, A. E. V. Neptunyl Pyrrophen Complexes: Exploring Schiff Base Chemistry with Multidentate Acyclic Ligands and Transuranics. *Chem. – Eur. J.* **2024**, *30*, e202402047. https://doi.org/10.1002/chem.202402047
74. Zhang, X.; Hrovat, D. A.; Borden, W. T. Calculations Predict That Carbon Tunneling Allows the Degenerate Cope Rearrangement of Semibullvalene to Occur Rapidly at Cryogenic Temperatures. *Org. Lett.* **2010**, *12*, 2798–2801. https://doi.org/10.1021/ol100879t.
75. Schleif, T.; Mieres-Perez, J.; Henkel, S.; Ertelt, M.; Borden, W. T.; Sander, W. The Cope Rearrangement of 1,5-Dimethylsemibullvalene-2(4)-d1: Experimental Evidence for Heavy-Atom Tunneling. *Angew. Chem.* **2017**, *129*, 10886–10889. https://doi.org/10.1002/ange.201704787.
76. Albright, T. R.; Winter, A. H. A Fine Line Separates Carbocations from Diradical Ions in Donor-Unconjugated Cations. *J. Am. Chem. Soc.* **2015**, *137*, 3402–3410. https://doi.org/10.1021/jacs.5b00707.
77. Takano, M.-a.; Abe, M. Photoreaction of 4-(Bromomethyl)-7-(diethylamino)coumarin: Generation of a Radical and Cation Triplet Diradical during the C–Br Bond Cleavage. *Org. Lett.* **2022**, *24*, 2804–2808. https://doi.org/10.1021/acs.orglett.2c00694.
78. Nguyen, H. D.; Abe, M. Crucial Roles of Leaving Group and Open-Shell Cation in Photoreaction of (Coumarin-4-yl)methyl Derivatives. *J. Am. Chem. Soc.* **2024**, *146*, 10993–11001. https://doi.org/10.1021/jacs.4c02880.
79. Falahati, K.; Tamura, H.; Burghardt, I.; Huix-Rotllant, M. Ultrafast Carbon Monoxide Photolysis and Heme Spin-Crossover in Myoglobin via Nonadiabatic Quantum Dynamics. *Nat. Commun.* **2018**, *9*, 4502. https://doi.org/10.1038/s41467-018-06615-1.
80. Barends, T. R. M.; Gorel, A.; Bhattacharyya, S.; Schirò, G.; Bacellar, C.; Cirelli, C.; Colletier, J.-P.; Foucar, L.; Grünbein, M. L.; Hartmann, E.; Hilpert, M.; Holton, J. M.; Johnson, P. J. M.; Kloos, M.; Knopp, G.; Marekha, B.; Nass, K.; Nass Kovacs, G.; Ozerov, D.; Stricker, M.; Weik, M.;

Doak, R. B.; Shoeman, R. L.; Milne, C. J.; Huix-Rotllant, M.; Cammarata, M.; Schlichting, I. Influence of Pump Laser Fluence on Ultrafast Myoglobin Structural Dynamics. *Nature* **2024**, *626*, 905–911. https://doi.org/10.1038/s41586-024-07032-9.

81. Loo, C. E.; Hix, M. A.; Wang, T.; Cisneros, G. A.; Kohli, R. M. Revealing Drivers for Carboxy-S-adenosyl-l-Methionine Use by Neomorphic Variants of a DNA Methyltransferase. *ACS Chem. Biol.* **2023**, *18*, 2224–2232. https://doi.org/10.1021/acschembio.3c00184.
82. Hix, M. A.; Wong, L.; Flath, B.; Chelico, L.; Cisneros, G. A. Single-Nucleotide Polymorphism of the DNA Cytosine Deaminase APOBEC3H Haplotype I Leads to Enzyme Destabilization and Correlates with Lung Cancer. *NAR Cancer* **2020**, *2*, zcaa023. https://doi.org/10.1093/narcan/zcaa023.
83. Rosales, A. R.; Wahlers, J.; Limé, E.; Meadows, R. E.; Leslie, K. W.; Savin, R.; Bell, F.; Hansen, E.; Helquist, P.; Munday, R. H.; Wiest, O.; Norrby, P.-O. Rapid Virtual Screening of Enantioselective Catalysts Using CatVS. *Nat. Catal.* **2019**, *2*, 41–45. https://doi.org/10.1038/s41929-018-0193-3.
84. Hansen, E.; Rosales, A. R.; Tutkowski, B.; Norrby, P.-O.; Wiest, O. Prediction of Stereochemistry using Q2MM. *Acc. Chem. Res.* **2016**, *49*, 996–1005. https://doi.org/10.1021/acs.accounts.6b00037.
85. Rosales, A. R.; Quinn, T. R.; Wahlers, J.; Tomberg, A.; Zhang, X.; Helquist, P.; Wiest, O.; Norrby, P.-O. Application of Q2MM to Predictions in Stereoselective Synthesis. *Chem. Commun.* **2018**, *54*, 8294–8311. https://doi.org/10.1039/C8CC03695K.
86. Grimme, S.; Bannwarth, C.; Shushkov, P. A Robust and Accurate Tight-Binding Quantum Chemical Method for Structures, Vibrational Frequencies, and Noncovalent Interactions of Large Molecular Systems Parametrized for All spd-Block Elements (Z = 1–86). *J. Chem. Theory Comput.* **2017**, *13*, 1989–2009. https://pubs.acs.org/doi/pdf/10.1021/acs.jctc.7b00118.
87. Katbashev, A.; Stahn, M.; Rose, T.; Alizadeh, V.; Friede, M.; Plett, C.; Steinbach, P.; Ehlert, S. Overview on Building Blocks and Applications of Efficient and Robust Extended Tight Binding. *J. Phys. Chem. A* **2025**, *129*, 2667–2682. https://doi.org/10.1021/acs.jpca.4c08263.
88. Grimme, S. Density Functional Theory with London Dispersion Corrections. *Wiley Interdiscip. Rev.: Comput. Mol. Sci.* **2011**, *1*, 211–228. https://doi.org/10.1002/wcms.30.
89. Cassidy, J. P.; Hofierka, J.; Cunningham, B.; Green, D. G. Many-Body Theory Calculations of Positronic-Bonded Molecular Dianions. *J. Chem. Phys.* **2024**, *160*, 084304. https://doi.org/10.1063/5.0188719.
90. Arthur-Baidoo, E.; Danielson, J. R.; Surko, C. M.; Cassidy, J. P.; Gregg, S. K.; Hofierka, J.; Cunningham, B.; Patterson, C. H.; Green, D. G. Positron Annihilation and Binding in Aromatic and Other Ring Molecules. *Phys. Rev. A* **2024**, *109*, 062801. https://doi.org/10.1103/PhysRevA.109.062801.